

Echo-enhanced molecular orientation at high temperaturesIlia Tutunnikov^{1,2,*}, Long Xu^{1,2,*}, Yehiam Prior^{1,2,†} and Ilya Sh. Averbukh^{1,2,‡}*AMOS and Department of Chemical and Biological Physics, The Weizmann Institute of Science, Rehovot 7610001, Israel*

(Received 15 August 2022; accepted 13 October 2022; published 8 December 2022)

We consider the orientation of linear and symmetric-top molecules induced by laser and delayed terahertz (THz) pulses at high rotational temperatures (up to room temperature). We introduce an echo-assisted approach in which the achieved transient molecular orientation is an order of magnitude higher than the orientation produced by a single THz pulse. The laser pulse first dissects the wide molecular phase-space distribution into multiple narrow strips (filaments), each being cold and evolving separately. A subsequent THz pulse causes a substantial transient orientation of the individual filaments, which leads to an enhanced orientation of the whole molecular ensemble at later times via the echo mechanism. This enhanced degree of orientation is important in attosecond science, chemical reaction control, ultrafast molecular imaging, and other domains of physics.

DOI: [10.1103/PhysRevA.106.L061101](https://doi.org/10.1103/PhysRevA.106.L061101)

Introduction. Diverse optical methods have been developed to align and orient molecules in the gas phase under field-free conditions [1,2]. A well-established route for orienting polar molecules is combining intense nonresonant laser fields with weak electrostatic fields [3–5]; another approach uses intense two-color laser pulses [6–14]. It is possible to induce enantioselective orientation in chiral molecules using laser pulses with twisted polarization [15–20]. Modern THz technology allows generating single- and half-cycle THz pulses to orient polar molecules under field-free conditions [21–27]. The efficiency of the methodologies mentioned above deteriorates rapidly with increasing rotational temperature due to the growing dispersion of the molecular angular velocities. At room temperature, the molecular orientation is typically just a few percent—too low for many practical applications.

Orienting molecules at room temperature without significant ionization is still an open, very challenging problem. Over the years, several proposals for enhancing molecular alignment and orientation have been put forward. These include applying optimized sequences of pulses [28–32], optimizing the pulses' parameters [33–37], and combining one-color laser pulses with two-color and THz pulses [38–43]. Several schemes were experimentally implemented and demonstrated improved orientation, mainly in the low-temperature regime [23,44].

In this Letter, we propose a general approach for overcoming the effect of thermal molecular rotational motion and for achieving significant field-free molecular orientation by moderate THz pulses at high temperatures (room temperature and higher). The method is based on a three-step process: (i) laser-induced dissection of the rotational phase-space distribution to narrow strips (filaments), (ii) subjecting all the filaments to the orienting action of a moderate THz pulse,

and (iii) waiting for the orientation echo induced by the two pulses to emerge after a delay. We show that the amplitude of the echo-induced orientation may be an order of magnitude higher than the orientation produced by the THz pulse alone at room temperature. The enhancement mechanism of the present work is related to the recently predicted and observed molecular alignment echoes [2,45,46]. In contrast to the spin echoes [47,48], they are based on the phenomenon of phase-space filamentation known in nonlinear systems (see, e.g., Refs. [49–52]).

Orientation by a single pulse. Consider a simplified planar rotor model, where noninteracting linear polar molecules (rigid rotors) are restricted to rotate in the XY plane and are subject to electromagnetic fields polarized along the X axis. The orienting light-molecule interaction potential is taken to be $\propto -\cos(\theta)$, where θ is the angle between the molecular axis and the X axis. Such a potential describes, e.g., the interaction of a single- or half-cycle THz pulse with the permanent molecular dipole. In the impulsive approximation (when the change in θ during the pulse is negligible), θ and the molecule's angular velocity ω after the orienting kick read

$$\theta(t) = \theta_0 + \omega t, \quad \omega = \omega_0 - P_{\text{or}} \sin(\theta_0), \quad (1)$$

where θ_0 and ω_0 are the initial angle and angular velocity, respectively. P_{or} is proportional to the orienting field amplitude $\varepsilon_{0,\text{or}}$ (for details, see Sec. I of the Supplemental Material [53]).

This orienting kick operates on molecules at nonzero rotational temperature, where the initial phase-space density of an isotropic ensemble of rotors is described by $p(\theta, \omega, t = 0) = (2\pi)^{-3/2} \sigma_T^{-1} \exp[-\omega_0^2/(2\sigma_T^2)]$ [see Fig. 1(a)]. The parameter $\sigma_T = \sqrt{k_B T/I}$ defines the thermal dispersion of angular velocities, where T is the temperature, k_B is the Boltzmann constant, and I is the moment of inertia. The degree of orientation of the molecular ensemble is quantified by the average value of $\cos(\theta)$, $\langle \cos(\theta) \rangle$. After the kick, $\langle \cos(\theta) \rangle(t) = \exp(-\sigma_T^2 t^2/2) J_1(P_{\text{or}} t)$ (for the derivation, see Sec. II A of the Supplemental Material [53]), where $J_1(z)$ is the Bessel function of the first kind of order one. When time is measured

*These authors contributed equally to this work.

†yehiam.prior@weizmann.ac.il

‡ilya.averbukh@weizmann.ac.il

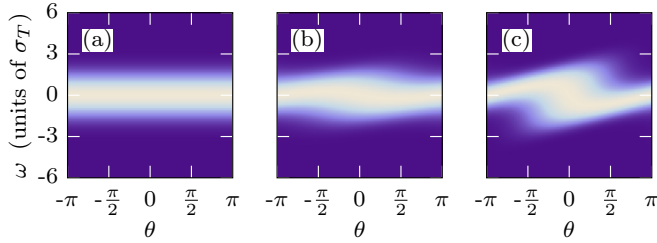


FIG. 1. Phase-space distribution for a single orienting pulse. (a) At $t = 0$, before the kick. After the kick at $t = \sigma_T^{-1}$ for (b) weak, $P_{\text{or}} = 0.25\sigma_T$, and (c) strong, $P_{\text{or}} = 0.75\sigma_T$, pulses.

in units of $1/\sigma_T$, the maximum degree of the kick-induced orientation is determined by a single dimensionless parameter, the ratio P_{or}/σ_T ($\propto \varepsilon_{0,\text{or}}/\sqrt{T}$). At room temperature, currently available THz pulses deform the phase-space distribution only weakly, and shortly after a kick, the phase-space density looks as it does in Fig. 1(b). For stronger kicks or at lower temperatures, the phase-space distribution folds as in Fig. 1(c), resulting in the higher orientation.

Phase-space filamentation. To help a weak orienting pulse overcome the detrimental effect of high temperatures, we stratify the rotational phase-space density into numerous separated strips (filaments). This way, the orienting pulse interacts with different molecular groups belonging to the individual narrow filaments rather than a single broad thermal distribution. For stratification, we use a relatively strong prepulse—a nonresonant linearly polarized laser pulse that precedes the orienting one. Intense laser pulses interacting with molecular polarizability have been widely used for inducing transient field-free molecular alignment [1,54–57], but here we focus on the postalignment dynamics leading to the phase-space filamentation [58–60].

A prepulse applied at $t = 0$ transforms the rotors’ variables according to

$$\theta(t) = \theta_0 + \omega t, \quad \omega = \omega_0 - P_{\text{pre}} \sin(2\theta_0), \quad (2)$$

where P_{pre} is proportional to the laser intensity (for details, see Sec. I of the Supplemental Material [53]). The phase-space density after the prepulse is described by

$$p(\theta, \omega, t) = \frac{\sigma_T^{-1}}{(2\pi)^{3/2}} \exp\left(-\frac{[\omega + P_{\text{pre}} \sin(2\theta - 2\omega t)]^2}{2\sigma_T^2}\right), \quad (3)$$

where we used Eq. (2) to express ω_0 in terms of ω and θ after the pulse, and substituted ω_0 into the Boltzmann distribution. With time, the phase-space density undergoes stratification and turns into a series of almost parallel filaments (strips) separated in angular velocity by π/t [see Eq. (3)]. Longer waiting times result in narrower filaments because the phase-space volume is conserved.

After some delay, at $t = \tau$, when the filaments are numerous and thin [see Fig. 2(a)], we apply the orienting kick. Since the dispersion of angular velocities within each filament is much smaller than the initial thermal dispersion, the interaction with the weak orienting pulse results in a non-negligible deformation of the filaments [see Fig. 2(b)]. With time, each filament folds as in Fig. 1(c), developing a bunch. Since the bunches move relative to each other (they are spaced apart by

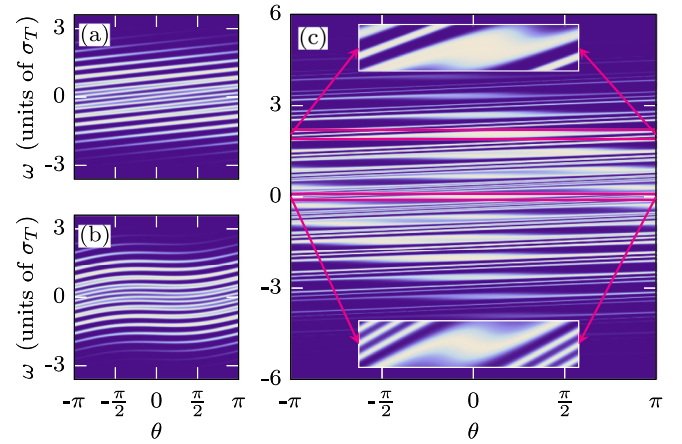


FIG. 2. Phase-space distribution. (a) Just before the orienting kick, $t = \tau_-$, for $\tau = 5/\sigma_T$. (b) Just after the orienting kick, $t = \tau_+$. (c) Orientation along the X axis, before the time of the orientation echo at $t = 3\tau$. Here, $P_{\text{pre}} = 2\sigma_T$, $P_{\text{or}} = 0.25\sigma_T$.

π/τ along the ω axis), no substantial orientation is visible just after the orienting kick. Nevertheless, due to the “quasiquantization” of the angular velocities, the bunches accumulate near $\theta = 0, \pi$ after an additional delay of τ (at $t \approx 2\tau$, not shown). A related mechanism is behind the alignment echoes previously observed in molecules gases [2,45,58–61], and similar echo phenomena in several other nonlinear systems [51,52,62–65].

After an additional delay of τ (at $t \approx 3\tau$), we witness another echo, and this is a different observation. The bunches resynchronize in an asymmetric manner resulting in molecular orientation. First, the bunches accumulate near $\theta = 0$ [just before $t = 3\tau$; see Fig. 2(c)], and then near $\theta = \pi$ (just after $t = 3\tau$, not shown). The closeups in Fig. 2(c) demonstrate that the bunches in each filament look similar to those seen in Fig. 1(c). Such resynchronizations happen again at later times, $t = 5\tau, 7\tau, \dots$, and manifest themselves in orientation echoes of higher orders [2,58–62].

Figure 3 shows the time-dependent orientation factor for two delays, $\tau = 10/\sigma_T$ and $\tau = 20/\sigma_T$. In both cases, the first orientation echo emerges at $t = 3\tau$. Compared to $\tau = 10/\sigma_T$, the echo amplitude for $\tau = 20/\sigma_T$ is significantly higher. In line with the qualitative arguments presented above, longer delays give rise to thinner filaments which, in turn, “help” the weak orienting kick.

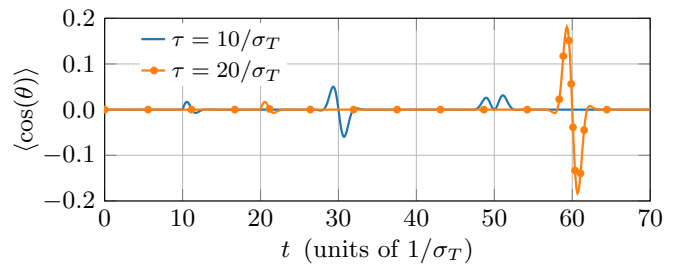


FIG. 3. Orientation factor following combined excitation by stratifying and orienting pulses. Here, $P_{\text{pre}} = 2\sigma_T$, $P_{\text{or}} = 0.1\sigma_T$. With the orienting pulse alone, the maximal orientation factor is ≈ 0.03 .

The degree of orientation in Fig. 3 can be analytically derived as follows. Just after the stratifying kick (laser prepulse), the rotor's variables are given by Eq. (2). After a delay equal to τ , at $t = \tau$, we apply the orienting kick which transforms the rotor's variables according to

$$\theta_2(t) = \theta_1(\tau) + (t - \tau)\omega_2, \quad \omega_2 = \omega_1 - P_{\text{or}} \sin[\theta_1(\tau)], \quad (4)$$

where θ_1 and ω_1 are the rotor's variables after the prepulse. The orientation factor is given by the real part of

$$\begin{aligned} \langle e^{i\theta} \rangle(t) &= \Theta(t - \tau)(2\pi)^{-3/2} \sigma_T^{-1} \\ &\times \int_{-\infty}^{\infty} \int_0^{2\pi} e^{i\theta_2(t)} e^{-\omega_0^2/(2\sigma_T^2)} d\theta_0 d\omega_0, \end{aligned} \quad (5)$$

where $\Theta(t - \tau)$ is the step function. After carrying out the integrals, the orientation signal reads (for the intermediate steps, see Sec. II B of the Supplemental Material [53])

$$\langle \cos(\theta) \rangle(t) = \Theta(t - \tau) \sum_{\text{odd } k} S_k(t), \quad (6)$$

where

$$S_k(t) = e^{-\sigma_T^2(t-k\tau)^2/2} J_k[P_{\text{or}}(t - \tau)] J_{\frac{k-1}{2}}[P_{\text{pre}}(k\tau - t)]. \quad (7)$$

The orientation signal consists of a series of pulsed responses separated in time by 2τ . The first orientation echo ($k = 3$, around $t = 3\tau$) is

$$S_3(t) \approx e^{-\sigma_T^2(t-3\tau)^2/2} J_3(2P_{\text{or}}\tau) J_1[P_{\text{pre}}(3\tau - t)]. \quad (8)$$

This expression shows the essential feature of the proposed scheme—for fixed temperature and stratifying kick (prepulse) strength, the echo amplitude increases with $P_{\text{or}}\tau$. In other words, increasing the delay τ is equivalent to increasing the orienting kick strength. The echo amplitude can be further enhanced by increasing P_{pre} (see Sec. II B of the Supplemental Material [53]). However, there is a limit to P_{pre} due to molecular ionization, which should be estimated for particular experimental conditions. Note that according to Eq. (8), while the overall echo duration is $\propto 1/\sigma_T = \sqrt{I/(k_B T)}$, the frequency of oscillations increases with P_{pre} . Thus, both temperature and the prepulse strength determine the effective duration of the significant orientation.

Classically, the delay τ could, in principle, be increased indefinitely to achieve a higher orientation factor. However, when the delay becomes comparable to the time of rotational quantum revivals [66,67], the interplay between echoes and revivals needs to be taken into account. As shown previously [64,68], a particular type of echo, termed a *quantum echo*, exists in the quantum case. A series of quantum echoes emerge on a long timescale, just before the quantum revivals. These echoes have a valuable property—in the limit of weak echo-inducing excitation (the orienting kick in our case), their amplitudes are higher than the classical echoes discussed.

To study the quantum echoes, we consider the dynamics of a kicked two-dimensional quantum rigid rotor (for details, see Sec. III of the Supplemental Material [53]). The rotational revival time is $T_{\text{rev}} = 4\pi I/\hbar$ [67]. Figure 4 shows the orientation factor in the presence of the stratifying (prepulse) and orienting kicks. Here, for demonstration purposes, we

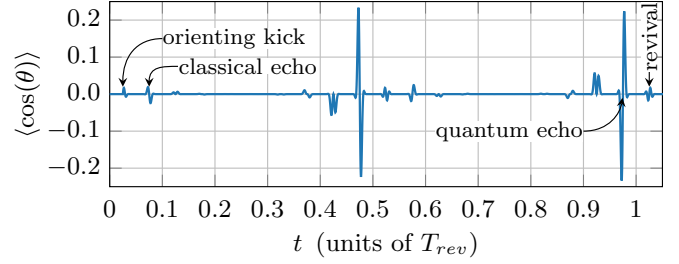


FIG. 4. Orientation factor calculated quantum mechanically at $T = 300$ K. Here, the orienting kick is applied at $\tau = 0.025T_{\text{rev}}$, which corresponds to $\tau \approx 7.2/\sigma_T$. The excitation strengths P_{pre} and P_{or} are the same as in Fig. 3. When only the orienting kick is applied, the maximal orientation factor is ≈ 0.03 .

choose a short time delay $\tau = 0.025T_{\text{rev}}$ resulting in a relatively weak classical orientation echo at $t = 3\tau = 0.075T_{\text{rev}}$. The amplitude of the classical echo is comparable to the maximal orientation factor induced by the orienting pulse alone, $\approx 3\%$. In striking contrast, a quantum echo emerges at a delay 2τ before the revival, at $t = 0.975T_{\text{rev}}$ with a much higher amplitude of $\approx 22\%$. Echoes of the same magnitude (but opposite sign) emerge just before the half revival. Alignment echoes emerging before the quantum revivals were studied both theoretically and experimentally [59,60].

Three-dimensional simulations. Next, we apply the developed understanding to three-dimensional linear and prolate symmetric-top molecules driven by the experimentally available femtosecond laser and picosecond THz fields. The rotational dynamics is treated classically and quantum mechanically within the rigid rotor approximation (for details, see Sec. IV of the Supplemental Material [53]). We model the time-dependent electric field, consisting of the delayed nonresonant laser and single-cycle THz pulses, using

$$\mathbf{E}(t) = \varepsilon_{\text{lsr}}(t) \cos(\omega_{\text{lsr}} t) \mathbf{e}_Z + \varepsilon_{\text{THz}}(t - \tau) \mathbf{e}_Z, \quad (9)$$

where ω_{lsr} is the carrier frequency of the laser pulse, $\varepsilon_{\text{lsr}}(t) = \varepsilon_{0,\text{lsr}} \exp[-2 \ln 2 (t/\sigma_{\text{lsr}})^2]$, $\varepsilon_{0,\text{lsr}}$ is the peak amplitude, and σ_{lsr} is the full width at half maximum (FWHM) of the laser pulse intensity profile. $\varepsilon_{\text{THz}}(t) = \varepsilon_{0,\text{THz}} (1 - 2\kappa t^2) \exp(-\kappa t^2)$ [25,69], where $\varepsilon_{0,\text{THz}}$ is the peak amplitude of the THz pulse and κ determines the temporal width of the THz pulse. τ is the time delay between the laser and THz pulses and \mathbf{e}_Z is a unit vector along the laboratory Z axis.

Linear molecule. We consider OCS as an example linear molecule. The molecular properties were taken from NIST [density functional theory (DFT), Coulomb-attenuating method with Becke three-parameter Lee-Yang-Parr functional and augmented correlation-consistent polarized valence triple zeta Gaussian basis set (CAM-B3LYP/aug-cc-pVTZ)] [70]: $I = 83.021 \text{ amu } \text{\AA}^2$, $\mu = 0.755 \text{ D}$, and $\Delta\alpha = 3.738 \text{ \AA}^3$. The rotational revival time of the OCS molecule is $T_{\text{rev}} = 2\pi I/\hbar \approx 82.4 \text{ ps}$ [67]. Figure 5 shows the time-dependent orientation factor obtained using classical and quantum simulations. Here, θ is the polar angle between the molecular axis and the polarization direction. The molecules were excited by the delayed laser and THz pulses [see Eq. (9)] at different initial rotational temperatures. The peak intensity of the laser

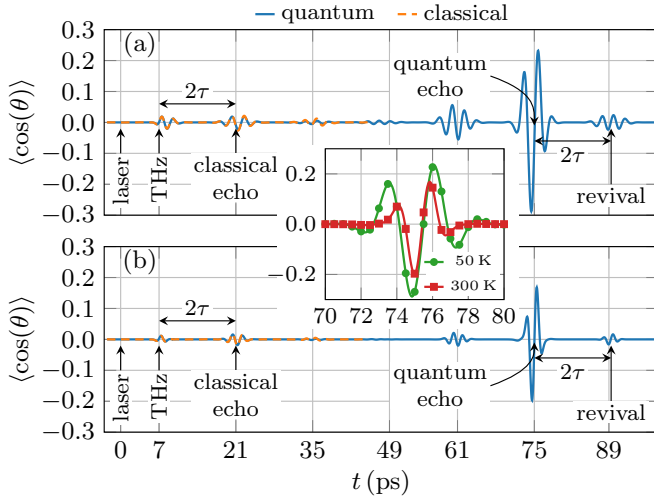


FIG. 5. Orientation factor for OCS molecules at (a) $T = 50$ K and (b) $T = 300$ K. The molecules are excited by delayed laser and THz pulses. The delay is $\tau = 7$ ps. The inset shows a magnified portion of the signal during the quantum echo. The maximum orientation factors obtained without the laser pulse are 0.0201 (50 K) and 0.0215 (300 K), respectively.

pulse is $I_{0,\text{lsr}} = 4 \times 10^{13}$ W/cm², and FWHM is $\sigma_{\text{lsr}} = 100$ fs. The THz pulse parameters are $\varepsilon_{0,\text{THz}} = 1.0$ MV/cm and $\kappa = 3.06$ ps⁻². Laser and THz pulses with similar parameters are readily available nowadays [71–74].

Both quantum and classical simulations demonstrate an immediate orientation response emerging during and shortly after the THz pulse excitation (at $t \approx 7$ ps). The first classical echo appears with a delay 2τ after the THz pulse, at $t \approx 21$ ps. The quantum mechanical result shows a strong echo signal before the orientation quantum revival, at $t \approx 75.4$ ps. The magnitude of this echo is an order of magnitude larger than the maximum orientation factor induced by a THz pulse alone. A significant orientation factor exceeding 10% (in absolute value) lasts for ≈ 1 ps for OCS molecules at 300 K (see the inset to Fig. 5). In agreement with previous studies [64,68] and the qualitative analysis based on the simplified models, the orientation during the quantum echo is significantly higher than the orientation during the classical echo.

Remarkably, the echo amplitude depends weakly on temperature (in the presented temperature range). This behavior can be understood with the help of the simplified model discussed above. The laser pulse is intense enough to induce efficient phase-space filamentation at the presented temperatures. With time, the number of filaments grows, and they become thinner. As a result, each molecular subgroup forming a single filament has a much reduced dispersion of angular velocities (originating from the initial thermal Boltzmann distribution), and it is effectively “cold.” Instead of competing with the highly dispersed angular velocities of the initial thermal ensemble, the weak THz pulse competes against the cold narrow filaments. When the change P_{or} of the rotation velocity due to the orienting pulse exceeds the width of the cold filaments, the following orientation echo dynamics becomes insensitive to this width and hence to the initial molecular temperature.

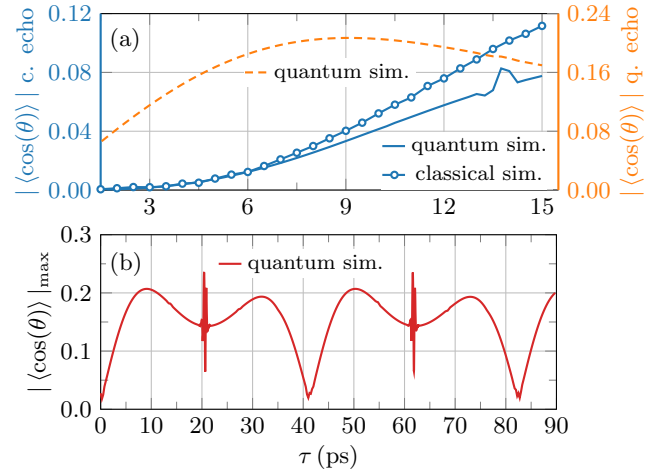


FIG. 6. Maximum orientation factors (OCS molecule, $T = 300$ K) as a function of τ . (a) During the classical echo (solid blue and blue circle) and during the quantum echo (orange dashed line). (b) The global maximum. The field parameters are the same as in Fig. 5. For comparison, the maximum orientation factor without the stratifying pulse is ≈ 0.0215 .

As discussed above, the echo amplitude increases with the time delay between the stratifying and orienting pulses (for fixed temperature and field parameters). Figure 6(a) shows the maximum orientation during the first classical echo (at delay 2τ after the THz pulse) and during the quantum echo (at delay 2τ before the orientation revival) for relatively short delays τ . For $\tau < 9$ ps, the magnitude of both types of orientation echoes increases with τ , which is consistent with the qualitative discussion above.

Figure 6(b) shows the global orientation maximum for various τ . The dependence on τ is periodic, and the period equal to half revival, $T_{\text{rev}}/2 \approx 41.2$ ps. When $\tau \approx T_{\text{rev}}/4$, the maximum degree of orientation exhibits high-amplitude oscillations. The reason for this high sensitivity is the coalescence of the echo that appears *after* the THz pulse at $t \approx 3\tau = 3T_{\text{rev}}/4$ and the echo that appears *before* the quantum revival at $t \approx T_{\text{rev}} - \tau = 3T_{\text{rev}}/4$. Notice, the orientation can be further enhanced using a stronger prepulse.

Previously, related schemes for enhancing the THz- and two-color-induced orientation were applied to cold OCS molecules (at 2 K in Ref. [23], and at 25 K in Ref. [44]). The orientation was substantially enhanced with the help of an aligning laser pulse. The delay between the aligning and orienting pulses was set to $T_{\text{rev}}/4$. The authors explained the enhancements using quantum mechanical arguments. Note that our results in Fig. 6 are in agreement with Refs. [23,44] for the specific delays of $T_{\text{rev}}/4$ and $3T_{\text{rev}}/4$.

Symmetric-top molecule. To demonstrate the robustness of the proposed orientation enhancement mechanism, we consider an additional example molecule CH₃I that belongs to the class of symmetric-top molecules. The molecular properties were taken from NIST [DFT, method CAM-B3LYP with pseudopotential (PP)-based correlation-consistent polarized valence triple zeta Gaussian basis set, cc-pVTZ-PP] [70]: $I_x = I_y \equiv I = 68.527$ amu Å², $I_z = 3.23$ amu Å², $\mu = 1.697$ D, and $\Delta\alpha = 2.951$ Å³.

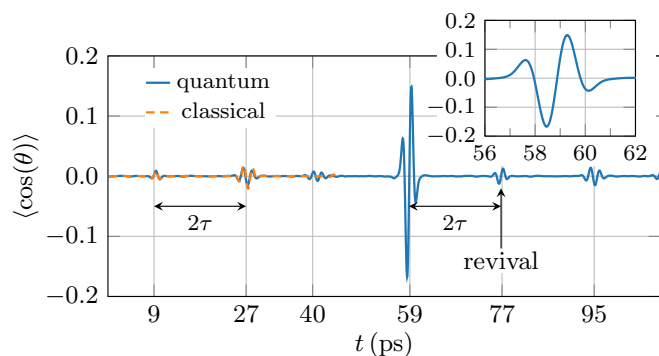


FIG. 7. Orientation factor for CH_3I molecules at $T = 300$ K. The delay between laser and THz pulses is $\tau = 9$ ps. The inset shows a magnified portion of the signal during the quantum echo. The maximum orientation factor obtained using only the THz pulse is ≈ 0.016 .

Figure 7 shows the orientation factor obtained using the quantum and classical simulations at room temperature. The field parameters are the same as in Fig. 5, except the lower THz field amplitude, $\epsilon_{0,\text{THz}} = 0.3$ MV/cm. On the short timescale, the quantum and classical results are close. The

maximum orientation emerges before the quantum revival (during the quantum echo). The maximum orientation obtained using the THz pulse alone at room temperature is ten times lower, $\approx 1.6\%$.

Conclusions. In this Letter, we addressed the open problem of how to orient room-temperature molecules with available moderate THz pulses. To overcome the detrimental effect of the thermal molecular rotations, we introduce a relatively strong nonresonant laser prepulse to dissect the broad phase-space distribution into multiple narrow filaments. The subsequent weak THz pulse induces several echoes of enhanced orientation at well-defined delays. The strongest of these echoes is the quantum echo observed at a delay 2τ before the orientation revival. In the presented examples, the maximum orientation at room temperature reaches tens of percent during the quantum echo. With stronger prepulses and various optimization procedures, even higher orientation is anticipated. The sizable orientation in a thermal gas paves the way to different imaging opportunities, chemical reaction control, and more.

Acknowledgments. L.X. acknowledges support from a Sir Charles Clore Postdoctoral Fellowship. This research was made possible in part by the historic generosity of the Harold Perlman Family.

- [1] C. P. Koch, M. Lemesko, and D. Sugny, Quantum control of molecular rotation, *Rev. Mod. Phys.* **91**, 035005 (2019).
- [2] K. Lin, I. Tutunnikov, J. Ma, J. Qiang, L. Zhou, O. Faucher, Y. Prior, I. Sh. Averbukh, and J. Wu, Spatiotemporal rotational dynamics of laser-driven molecules, *Adv. Photonics* **2**, 024002 (2020).
- [3] B. Friedrich and D. Herschbach, Enhanced orientation of polar molecules by combined electrostatic and nonresonant induced dipole forces, *J. Chem. Phys.* **111**, 6157 (1999).
- [4] B. Friedrich and Herschbach, Manipulating molecules via combined static and laser fields, *J. Phys. Chem. A* **103**, 10280 (1999).
- [5] H. Sakai, S. Minemoto, H. Nanjo, H. Tanji, and T. Suzuki, Controlling the Orientation of Polar Molecules with Combined Electrostatic and Pulsed, Nonresonant Laser Fields, *Phys. Rev. Lett.* **90**, 083001 (2003).
- [6] T. Kanai and H. Sakai, Numerical simulations of molecular orientation using strong, nonresonant, two-color laser fields, *J. Chem. Phys.* **115**, 5492 (2001).
- [7] S. De, I. Znakovskaya, D. Ray, F. Anis, N. G. Johnson, I. A. Bocharova, M. Magrakvelidze, B. D. Esry, C. L. Cocke, I. V. Litvinyuk, and M. F. Kling, Field-Free Orientation of CO Molecules by Femtosecond Two-Color Laser Fields, *Phys. Rev. Lett.* **103**, 153002 (2009).
- [8] K. Oda, M. Hita, S. Minemoto, and H. Sakai, All-Optical Molecular Orientation, *Phys. Rev. Lett.* **104**, 213901 (2010).
- [9] J. Wu and H. Zeng, Field-free molecular orientation control by two ultrashort dual-color laser pulses, *Phys. Rev. A* **81**, 053401 (2010).
- [10] E. Frumker, C. T. Hebeisen, N. Kajumba, J. B. Bertrand, H. J. Wörner, M. Spanner, D. M. Villeneuve, A. Naumov, and P. B. Corkum, Oriented Rotational Wave-Packet Dynamics Studies via High Harmonic Generation, *Phys. Rev. Lett.* **109**, 113901 (2012).
- [11] M. Spanner, S. Patchkovskii, E. Frumker, and P. Corkum, Mechanisms of Two-Color Laser-Induced Field-Free Molecular Orientation, *Phys. Rev. Lett.* **109**, 113001 (2012).
- [12] I. Znakovskaya, M. Spanner, S. De, H. Li, D. Ray, P. Corkum, I. V. Litvinyuk, C. L. Cocke, and M. F. Kling, Transition between Mechanisms of Laser-Induced Field-Free Molecular Orientation, *Phys. Rev. Lett.* **112**, 113005 (2014).
- [13] K. Lin, I. Tutunnikov, J. Qiang, J. Ma, Q. Song, Q. Ji, W. Zhang, H. Li, F. Sun, X. Gong, H. Li, P. Lu, H. Zeng, Y. Prior, I. Sh. Averbukh, and J. Wu, All-optical field-free three-dimensional orientation of asymmetric-top molecules, *Nat. Commun.* **9**, 5134 (2018).
- [14] L. Xu, I. Tutunnikov, Y. Prior, and I. Sh. Averbukh, Long-lasting orientation of symmetric-top molecules excited by two-color femtosecond pulses, *Front. Phys.* **9**, 689635 (2021).
- [15] A. Yachmenev and S. N. Yurchenko, Detecting Chirality in Molecules by Linearly Polarized Laser Fields, *Phys. Rev. Lett.* **117**, 033001 (2016).
- [16] E. Gershnel and I. Sh. Averbukh, Orienting Asymmetric Molecules by Laser Fields with Twisted Polarization, *Phys. Rev. Lett.* **120**, 083204 (2018).
- [17] A. A. Milner, J. A. M. Fordyce, I. MacPhail-Bartley, W. Wasserman, V. Milner, I. Tutunnikov, and I. Sh. Averbukh, Controlled Enantioselective Orientation of Chiral Molecules with an Optical Centrifuge, *Phys. Rev. Lett.* **122**, 223201 (2019).
- [18] I. Tutunnikov, J. Floß, E. Gershnel, P. Brumer, and I. Sh. Averbukh, Laser-induced persistent orientation of chiral molecules, *Phys. Rev. A* **100**, 043406 (2019).
- [19] I. Tutunnikov, J. Floß, E. Gershnel, P. Brumer, I. Sh. Averbukh, A. A. Milner, and V. Milner, Observation of

- persistent orientation of chiral molecules by a laser field with twisted polarization, *Phys. Rev. A* **101**, 021403(R) (2020).
- [20] L. Xu, Enantioselective chiral orientation induced by a combination of a long and a short laser pulse, *Phys. Rev. A* **105**, 033113 (2022).
- [21] S. Fleischer, Y. Zhou, R. W. Field, and K. A. Nelson, Molecular Orientation and Alignment by Intense Single-Cycle THz Pulses, *Phys. Rev. Lett.* **107**, 163603 (2011).
- [22] K. Kitano, N. Ishii, N. Kanda, Y. Matsumoto, T. Kanai, M. Kuwata-Gonokami, and J. Itatani, Orientation of jet-cooled polar molecules with an intense single-cycle THz pulse, *Phys. Rev. A* **88**, 061405(R) (2013).
- [23] K. N. Egodapitiya, S. Li, and R. R. Jones, Terahertz-Induced Field-Free Orientation of Rotationally Excited Molecules, *Phys. Rev. Lett.* **112**, 103002 (2014).
- [24] R. Damari, S. Kallush, and S. Fleischer, Rotational Control of Asymmetric Molecules: Dipole- versus Polarizability-Driven Rotational Dynamics, *Phys. Rev. Lett.* **117**, 103001 (2016).
- [25] P. Babilotte, K. Hamraoui, F. Billard, E. Hertz, B. Lavorel, O. Faucher, and D. Sugny, Observation of the field-free orientation of a symmetric-top molecule by terahertz laser pulses at high temperature, *Phys. Rev. A* **94**, 043403 (2016).
- [26] L. Xu, I. Tutunnikov, E. Gershnel, Y. Prior, and I. Sh. Averbukh, Long-Lasting Molecular Orientation Induced by a Single Terahertz Pulse, *Phys. Rev. Lett.* **125**, 013201 (2020).
- [27] A. Beer, R. Damari, Y. Chen, and S. Fleischer, Molecular orientation-induced second-harmonic generation: Deciphering different contributions apart, *J. Phys. Chem. A* **126**, 3732 (2022).
- [28] M. Leibscher, I. Sh. Averbukh, and H. Rabitz, Molecular Alignment by Trains of Short Laser Pulses, *Phys. Rev. Lett.* **90**, 213001 (2003).
- [29] C. Z. Bisgaard, M. D. Poulsen, E. Péronne, S. S. Viftrup, and H. Stapelfeldt, Observation of Enhanced Field-Free Molecular Alignment by Two Laser Pulses, *Phys. Rev. Lett.* **92**, 173004 (2004).
- [30] K. F. Lee, I. V. Litvinyuk, P. W. Dooley, M. Spanner, D. M. Villeneuve, and P. B. Corkum, Two-pulse alignment of molecules, *J. Phys. B: At., Mol. Opt. Phys.* **37**, L43 (2004).
- [31] D. Pinkham, K. E. Mooney, and R. R. Jones, Optimizing dynamic alignment in room temperature CO, *Phys. Rev. A* **75**, 013422 (2007).
- [32] X.-M. Zhang, J. Li, J. Yu, and S.-L. Cong, Field-free molecular orientation induced by a Single-cycle THz laser pulse train, *Commun. Comput. Phys.* **20**, 689 (2016).
- [33] J. H. Mun and H. Sakai, Improving molecular orientation by optimizing relative delay and intensities of two-color laser pulses, *Phys. Rev. A* **98**, 013404 (2018).
- [34] X.-F. Yu and S. Wang, Molecular orientation of thermal ensemble induced by two-color slow turn-on and rapid turn-off laser pulses, *Chem. Phys. Lett.* **784**, 139085 (2021).
- [35] Md. Maruf Hossain, X. Zhang, S. Minemoto, and H. Sakai, Stronger orientation of state-selected OCS molecules with relative-delay-adjusted nanosecond two-color laser pulses, *J. Chem. Phys.* **156**, 041101 (2022).
- [36] S. Wang and N. E. Henriksen, Optimal field-free molecular orientation with nonresonant two-color adiabatic-turn-on and sudden-turn-off laser pulses, *Phys. Rev. A* **102**, 063120 (2020).
- [37] L. Xu, I. Tutunnikov, Y. Prior, and I. Sh. Averbukh, Optimization of the double-laser-pulse scheme for enantioselective orientation of chiral molecules, *J. Chem. Phys.* **157**, 034304 (2022).
- [38] M. Spanner, E. A. Shapiro, and M. Ivanov, Coherent Control of Rotational Wave-Packet Dynamics via Fractional Revivals, *Phys. Rev. Lett.* **92**, 093001 (2004).
- [39] D. Daems, S. Guérin, D. Sugny, and H. R. Jauslin, Efficient and Long-Lived Field-Free Orientation of Molecules by a Single Hybrid Short Pulse, *Phys. Rev. Lett.* **94**, 153003 (2005).
- [40] E. Gershnel, I. Sh. Averbukh, and R. J. Gordon, Orientation of molecules via laser-induced antialignment, *Phys. Rev. A* **73**, 061401(R) (2006); Enhanced molecular orientation induced by molecular antialignment, *ibid.* **74**, 053414 (2006).
- [41] K. Kitano, N. Ishii, and J. Itatani, High degree of molecular orientation by a combination of THz and femtosecond laser pulses, *Phys. Rev. A* **84**, 053408 (2011).
- [42] R. Tehini, M. Z. Hoque, O. Faucher, and D. Sugny, Field-free molecular orientation of $^1\Sigma$ and $^2\Pi$ molecules at high temperature, *Phys. Rev. A* **85**, 043423 (2012).
- [43] Y. Liu, J. Li, J. Yu, and S.-L. Cong, Field-free molecular orientation by two-color shaped laser pulse together with time-delayed THz laser pulse, *Laser Phys. Lett.* **10**, 076001 (2013).
- [44] K. Sonoda, A. Iwasaki, K. Yamanouchi, and H. Hasegawa, Field-free molecular orientation of nonadiabatically aligned OCS, *Chem. Phys. Lett.* **693**, 114 (2018).
- [45] L. Xu, I. Tutunnikov, L. Zhou, K. Lin, J. Qiang, P. Lu, Y. Prior, I. Sh. Averbukh, and J. Wu, Echoes in unidirectionally rotating molecules, *Phys. Rev. A* **102**, 043116 (2020).
- [46] J. Ma, L. H. Coudert, F. Billard, M. Bournazel, B. Lavorel, J. Wu, G. Maroulis, J.-M. Hartmann, and O. Faucher, Echo-assisted impulsive alignment of room-temperature acetone molecules, *Phys. Rev. Res.* **3**, 023192 (2021).
- [47] E. L. Hahn, Spin Echoes, *Phys. Rev.* **80**, 580 (1950).
- [48] E. L. Hahn, Free nuclear induction, *Phys. Today* **6**(11), 4 (1953).
- [49] D. Lynden-Bell, Statistical mechanics of violent relaxation in stellar systems, *Mon. Not. R. Astron. Soc.* **136**, 101 (1967).
- [50] G. Guignard, Phase space dynamics, in *Frontiers of Particle Beams*, edited by M. Month and S. Turner (Springer, Berlin, 1988), pp. 1–50.
- [51] G. V. Stupakov, Echo effect in hadron colliders, U.S. DOE Technical Report No. SSCL-579, Superconducting Super Collider Laboratory, Texas (1992).
- [52] G. Stupakov, *Handbook of Accelerator Physics and Engineering*, 2nd ed., edited by A. W. Chau *et al.* (World Scientific, Singapore, 2013), Chap. 2.3.13, pp. 121–123.
- [53] See Supplemental Material at <http://link.aps.org/supplemental/10.1103/PhysRevA.106.L061101> for the interaction within the impulsive approximation (Sec. I), for the derivation of the orientation factor in the two-dimensional classical model (Sec. II), for the description of two-dimensional quantum rigid rotor (Sec. III), as well as for the further details on the three-dimensional simulations (Sec. IV).
- [54] H. Stapelfeldt and T. Seideman, Colloquium: Aligning molecules with strong laser pulses, *Rev. Mod. Phys.* **75**, 543 (2003).
- [55] Y. Ohshima and H. Hasegawa, Coherent rotational excitation by intense nonresonant laser fields, *Int. Rev. Phys. Chem.* **29**, 619 (2010).
- [56] S. Fleischer, Y. Khodorkovsky, E. Gershnel, Y. Prior, and I. Sh. Averbukh, Molecular alignment induced by ultrashort laser

- pulses and its impact on molecular motion, *Isr. J. Chem.* **52**, 414 (2012).
- [57] M. Lemesko, R. V. Krems, J. M. Doyle, and S. Kais, Manipulation of molecules with electromagnetic fields, *Mol. Phys.* **111**, 1648 (2013).
- [58] G. Karras, E. Hertz, F. Billard, B. Lavorel, J.-M. Hartmann, O. Faucher, E. Gershnel, Y. Prior, and I. Sh. Averbukh, Orientation and Alignment Echoes, *Phys. Rev. Lett.* **114**, 153601 (2015).
- [59] K. Lin, P. Lu, J. Ma, X. Gong, Q. Song, Q. Ji, W. Zhang, H. Zeng, J. Wu, G. Karras, G. Siour, J.-M. Hartmann, O. Faucher, E. Gershnel, Y. Prior, and I. Sh. Averbukh, Echoes in Space and Time, *Phys. Rev. X* **6**, 041056 (2016).
- [60] K. Lin, J. Ma, X. Gong, Q. Song, Q. Ji, W. Zhang, H. Li, P. Lu, H. Li, H. Zeng, J. Wu, J.-M. Hartmann, O. Faucher, E. Gershnel, Y. Prior, and I. Sh. Averbukh, Rotated echoes of molecular alignment: Fractional, high order and imaginary, *Opt. Express* **25**, 24917 (2017).
- [61] G. Karras, E. Hertz, F. Billard, B. Lavorel, G. Siour, J.-M. Hartmann, O. Faucher, E. Gershnel, Y. Prior, and I. Sh. Averbukh, Experimental observation of fractional echoes, *Phys. Rev. A* **94**, 033404 (2016).
- [62] D. Xiang and G. Stupakov, Echo-enabled harmonic generation free electron laser, *Phys. Rev. ST Accel. Beams* **12**, 030702 (2009).
- [63] J. Qiang, I. Tutunnikov, P. Lu, K. Lin, W. Zhang, F. Sun, Y. Silberberg, Y. Prior, I. Sh. Averbukh, and J. Wu, Echo in a single vibrationally excited molecule, *Nat. Phys.* **16**, 328 (2020).
- [64] I. Tutunnikov, K. V. Rajitha, and I. Sh. Averbukh, Echoes in a single quantum Kerr-nonlinear oscillator, *Phys. Rev. A* **103**, 013717 (2021).
- [65] I. Tutunnikov, K. V. Rajitha, A. Y. Voronin, V. V. Nesvizhevsky, and I. Sh. Averbukh, Impulsively Excited Gravitational Quantum States: Echoes and Time-Resolved Spectroscopy, *Phys. Rev. Lett.* **126**, 170403 (2021).
- [66] I. Sh. Averbukh and N. F. Perelman, Fractional revivals: Universality in the long-term evolution of quantum wave packets beyond the correspondence principle dynamics, *Phys. Lett. A* **139**, 449 (1989).
- [67] R. W. Robinett, Quantum wave packet revivals, *Phys. Rep.* **392**, 1 (2004).
- [68] M. Herrera, T. M. Antonsen, E. Ott, and S. Fishman, Echoes and revival echoes in systems of anharmonically confined atoms, *Phys. Rev. A* **86**, 023613 (2012).
- [69] P. Babilotte, L. H. Coudert, F. Billard, E. Hertz, O. Faucher, and B. Lavorel, Experimental and theoretical study of free induction decay of water molecules induced by terahertz laser pulses, *Phys. Rev. A* **95**, 043408 (2017).
- [70] R. D. Johnson, NIST Computational Chemistry Comparison and Benchmark Database, Release 20 (2019), <http://cccbdb.nist.gov>.
- [71] M. Clerici, M. Peccianti, B. E. Schmidt, L. Caspani, M. Shalaby, M. Giguère, A. Lotti, A. Couairon, F. Légaré, T. Ozaki, D. Faccio, and R. Morandotti, Wavelength Scaling of Terahertz Generation by Gas Ionization, *Phys. Rev. Lett.* **110**, 253901 (2013).
- [72] T. I. Oh, Y. J. Yoo, Y. S. You, and K. Y. Kim, Generation of strong terahertz fields exceeding 8 MV/cm at 1 kHz and real-time beam profiling, *Appl. Phys. Lett.* **105**, 041103 (2014).
- [73] C. Vicario, A. V. Ovchinnikov, S. I. Ashitkov, M. B. Agranat, V. E. Fortov, and C. P. Hauri, Generation of 0.9-mJ THz pulses in DSTMS pumped by a Cr:Mg₂SiO₄ laser, *Opt. Lett.* **39**, 6632 (2014).
- [74] M. Shalaby and C. P. Hauri, Demonstration of a low-frequency three-dimensional terahertz bullet with extreme brightness, *Nat. Commun.* **6**, 5976 (2015).